Flow Turbulence Combust (2012) 88:169–189
DOI 10.1007/s10494-011-9357-9

LES Investigation of the Flow Through an Effusion-Cooled Aeronautical Combustor Model

Emmanuel Motheau · Thomas Lederlin · Juan L. Florenciano · Pascal Bruel

Received: 14 October 2010 / Accepted: 14 June 2011 / Published online: 5 July 2011

Abstract The present study is devoted to the analysis of the behaviour of the flow through an effusion-cooled aeronautical combustor model. High-fidelity calculations are performed on an experimental model of a combustion chamber multi-perforated wall and compared to experimental measurements. The effect of combustion instability on the effusion-cooling system is investigated by studying the interaction of an acoustic wave with the jets-in-crossflow issued from the cooling plate. It is shown that the mass-flow rate through the plate can be drastically reduced by the acoustic wave, which demonstrates the destructive effect that such instability may have on the cooling of an aeronautical combustion chamber.

Keywords LES · Effusion-cooling · Wall-bounded flows · Acoustic forcing · Jet-in-crossflow

1 Industrial and Scientific Motivations

To increase the lifespan of an aeronautical gas turbine combustor, the walls of the flame tube must be protected against the high surrounding temperature. Many

E. Motheau (✉) · T. Lederlin · J. L. Florenciano
Turbomeca S.A., 64511, Bordes Cedex, France
e-mail: emmanuel.motheau@cerfacs.fr

T. Lederlin
e-mail: thomas.lederlin@turbomeca.fr

J. L. Florenciano
e-mail: juan-luis.florenciano-merino@turbomeca.fr

P. Bruel
CNRS & Université de Pau et des Pays de l'Adour Laboratoire de Mathématiques et de leurs Applications, IPRA, BP 1155, 64000, Pau Cedex, France
e-mail: pascal.bruel@univ-pau.fr

cooling techniques were developed throughout the evolution of gas turbines, the most recent relying on the use of effusion (or transpiration) cooling. This technique has several advantages, in terms of efficiency and ease of manufacturing, over classical techniques such as Z-rings or ceramic coating.

The cooling effectiveness of an effusion-cooling plate depends on several parameters, such as hole spacing, angle, diameter, conicalness, etc. and must be precisely known by the combustor designers. The use of cleaner and more efficient injection technology makes modern engines more and more prone to thermoacoustic instability and the impact of this phenomenon on the performance of an effusion-cooling plate also needs to be investigated.

As the typical size of a transpiration-cooling plate hole is below one millimeter, it is still impossible to include all the geometrical details of the multi-perforated plates in a combustor simulation. As a consequence, homogeneous boundary-condition models for simulating flows around effusion-cooling plates are commonly used in RANS and LES. The development of those models requires detailed experimental and numerical studies on such flow configurations.

Previous TURBOMECA activities in that domain have been undertaken with the work of Miron [14] and Most [15]. The experimental test bench "MAVERIC" developed at University of Pau (UPPA) in close partnership with TURBOMECA was used to perform velocity measurements of an airflow through an effusion-cooling plate at scale 12.5:1. The experimental results have been used by Most [15] to validate RANS calculations involving different types of holes (circular and cone-shaped), and by Mendez and Nicoud [13] for large-eddy simulations (LES) of jets through circular holes in the case of an infinite plate.

The present work deals with LES of a jets in crossflow configuration. Convergent cone-shaped holes arranged in a pattern that mimics that used for an aeronautical combustion chamber wall were chosen. All the geometrical details of the plate are taken into account in the simulation. The properties of the parietal flow resulting from the interactions between the jets and the crossflow are investigated. Wall-bounded flows as the ones presently investigated are well-known for being the most difficult to capture in LES, especially in the case of complex geometries, for which it is too costly to refine the computational grid to a size that permits to resolve the energy-containing eddies. In his study, Chapman [4] showed that the grid-resolution requirements for the LES of turbulent boundary layers were as stringent as for direct numerical simulation (DNS), which is an obstacle to apply LES for quite a lot of engineering flows of interest.

To overcome these prohibitive near-wall resolution requirements, several wall stress models are designed to reproduce first order statistics so as to catch the logarithmic law of the wall. A detailed review of several methods and models can be found in the works of Templeton et al. [24] and Piomelli et al. [18]. The main common property of algebraic and two-layer wall models is that the wall stresses are prescribed on the wall-parallel velocity components, while the wall-normal velocity is set to zero. This assumption is important when computing complex wall bounded flow configurations, especially at corners where ambiguities may arise to determine the flow direction when using cell vertex based finite volume methods.

As recalled by Nicoud et al. [17], the problem of wall-stress modelling is inherently coupled to the sub-grid scale model because the filter width is always larger than the local turbulent integral length scales at the wall. The sub-grid scale model frequently

used in LES of realistic configurations is the Smagorinsky model [22], which is known to poorly represent the sub-grid Reynolds stresses near a wall [1]. Nicoud and Ducros [16] proposed a Wall-Adaptating Local Eddy-viscosity (WALE) model, based on a tensor invariant and reproducing the proper scaling of the viscosity at the wall. The interest of the WALE model is that the turbulent viscosity effect goes naturally to zero at the wall, thus no law of the wall is required as a boundary condition. Moreover, the model is invariant to any coordinate translation or rotation, so that it is well-suited for LES in complex flow configurations as no specific numerical strategy is needed to specify the direction of the flow at corners.

In the first part of the present study, the impact of wall modelling on the LES of an effusion-cooling film is investigated. The WALE model with a zero-velocity treatment at the walls is tested and compared to the standard Smagorinsky model with a classical wall law function. Different levels of pressure difference across the effusion-cooling plate are investigated, thus giving an insight into the flow behaviour at different regimes of the jets-crossflow interaction.

After validation of these pulsation free flow simulations, an acoustic pulsation is introduced in the crossflow. The jets issued from the plate are acoustically excited by the standing wave which modifies their vortical structure. The effect of this interaction on the cooling flow rate helps to anticipate the impact that the presence of an acoustic mode standing in a combustor might have on the wall cooling efficiency.

The sensitivity of turbulent jets to an acoustic forcing has been largely studied in the free-jet case [6, 7, 9]. In 1971, Crow and Champagne [7] discovered that the shear-layer of a jet can support orderly vortical structures and operates as a finely tuned amplifier of upstream disturbances. The perturbation of jets can be explained by the faculty of acoustic waves to excite the unstable modes of the flow [6]. Since the jet in crossflow (JICF) instability modes are significantly different from those of the free jets [12], the JICF response to an acoustic excitation and the resulting sensitivity of an effusion-cooling flow are also very specific and need to be studied.

Recently, DNS based global stability studies of a normal jet in crossflow configuration have been performed by Bagheri et al. [2, 21]. These authors showed the self-sustained oscillating character of the flow and concluded that the steady flow consists mainly of a steady counter-rotating vortex pair (CVP) and horseshoe-shaped vortices close to the wall. High-frequency unstable global eigenmodes associated with shear-layer instabilities on the CVP and low-frequency modes associated with shedding vortices in the wake of the jet were also identified.

Effusion cooling flows represent a particular class of the academic JICF configuration studied in previous works [8, 12] . The main differences are: effusion cooling holes are conical-shaped, the injection direction in combustor wall is not perpendicular to main stream direction and jet velocity profile at any hole exit section is not axisymmetric. The authors' interest is to set up a starting point by addressing the following aspects:

– Validation of a numerical methodology to simulate an effusion cooling flow in the presence of a standing acoustic wave in the main flow.
– Investigation of vortical passage frequencies on mixing layers in the particular case of effusion cooling jets.

The response of turbulent jets to an acoustic excitation depends on all the forcing parameters, however the aim of this preliminary study is not to carry out a

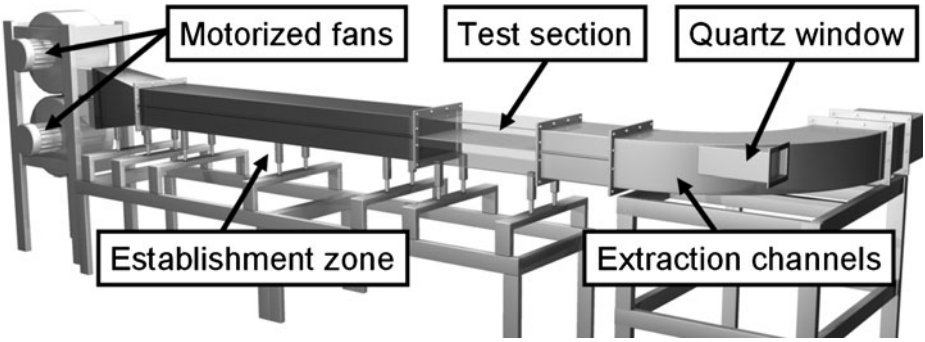

Fig. 1 The experimental test facility

parametrical analysis of the effusion cooling sensitivity to acoustic forcing, this item will be tackled in future works.

2 Experimental Set-up

An overview of the test facility MAVERIC from which the data are taken is presented in Fig. 1. It consists basically of two 2.5 m long superimposed channels of identical rectangular 400 mm (width) × 120 mm (height) cross-section followed by a 800 mm long Plexiglas-made test section with a similar cross-section and which accommodates a removable perforated plate. The test section is followed by the exhaust section which evacuates the air flows outside through the lateral wall of the room. The two air-streams are generated by two centrifugal fans powered by two 1 KW electrical motors controlled by two Siemens Micro-Master MC420 inverters. In order to generate a pressure difference between the two streams, a pressure loss plate is placed normally to the lower flow. The level of the pressure difference is controlled by the porosity of the pressure loss plate and the flow rate of the lower stream.

Thanks to the pressure difference, some air from the lower channel is passing into the upper flow through the multiperforated plate. The test section is mostly transparent (Plexiglass) and a quartz window is fitted at the level of the upper extraction channel allowing for a great flexibility in the use of laser diagnostics at the plate location, such as laser Doppler velocimetry (LDV) or particle image velocimetry (PIV).

The shape of the up-scaled holes was chosen in order to mimic that of the holes of a real TURBOMECA combustion chamber. Since the drilling process of the chamber holes uses a laser beam technique, the resulting hole shape is not cylindrical and

Table 1 Geometrical parameters of the effusion-cooling plate model

Equivalent diameter	d_{ref}
Hole inlet diameters	$3d_{\text{ref}} \times 1.5d_{\text{ref}}$
Hole exit diameters	$2d_{\text{ref}} \times d_{\text{ref}}$
L	$7d_{\text{ref}}$
P	$16d_{\text{ref}}$

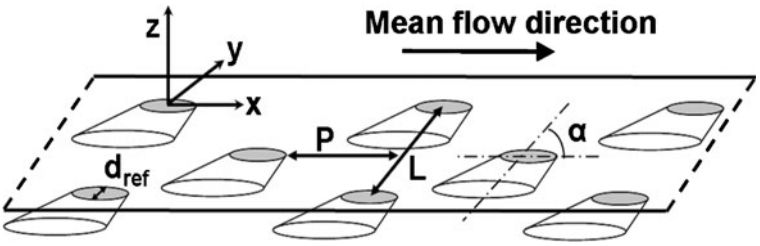

Fig. 2 Multi-perforated plate pattern

proves to be approximately conical, yielding elliptical inlet and exit hole sections. Table 1 summarizes the dimensions at scale 12.5:1 of the elliptical hole sections, the lateral spacing L between two successive holes in a row, and the longitudinal spacing P between two rows. Dimensions are expressed with the use of a reference diameter d_{ref} defined as the small diameter of the elliptic exit section. The angle of inclination between the hole axis and the plate in the axial direction (see Fig. 2) is around $\alpha \approx 30$ deg. The estimated dispersion over all the plate holes is estimated to be $\pm 2\%$ in the holes dimensions and locations and $\pm 0.5\%$ in α.

Table 2 summarizes the main flow parameters that have been investigated so far on the MAVERIC test facility [15]. A blowing parameter $\mathcal{M}$ is defined by the ratio $\overline{U}_{\text{jet}}/U_{\max}$ where $\overline{U}_{\text{jet}}$ is the mean velocity taken at the exit of a hole and $U_{\max}$ is the maximum of the axial velocity profile at the upper-channel inlet.

It must be mentioned that if the Reynolds number of the crossflow given in Table 2 is fairly equivalent to that found at scale 1 (i.e. in a real combustion chamber), the values of the blowing parameter $\mathcal{M}$ are noticeably lower since the ratio is approximately of 1 (scale 12.5) to 5 (scale 1). It is believed though that these two 12.5-scale flow configurations are relevant for performing LES validation since most of the well-known prominent features of such a multi-jet in crossflow configuration are already present [14, 15].

3 Numerical Set-up

In the present work, large-eddy simulations are performed with the AVBP code (Advanced Virtual Burner Project), developed at CERFACS (Toulouse, France) and IFP (the French Petroleum Institute). AVBP is a parallel CFD code that solves the laminar and turbulent compressible Navier-Stokes equations in two and

Table 2 Flow parameters for cases 1 and 2

Case		1	2
$\Delta P(Pa)$		45	136
$U_{\max}$ (m/s)	Upper channel	4.5	4.5
	Lower channel	2.26	3.78
Reynolds number	Upper channel	35,500	35,500
	Lower channel	18,000	30,000
Blowing parameter $\mathcal{M}$		1.34	2.3

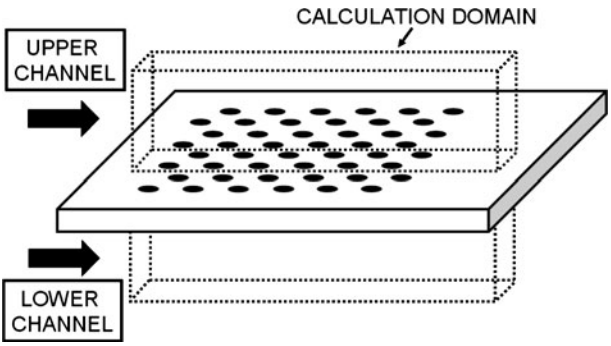

Fig. 3 Periodic calculation domain

three space dimensions on unstructured and hybrid grids. Originally devoted to the computation of reactive flows in combustors (see for example Wolf et al. [25] and Boileau et al. [3]), AVBP has also been extensively validated in the case of pure aerodynamics by Prière et al. [20] and Mendez and Nicoud [13].

A third order, Taylor–Galerkin type, scheme developed by Colin [5] is used for both time and space advancement. Boundary conditions are implemented through the NSCBC formulation derived by Poinsot and Lele [19]. Two different subgrid-scale models have been investigated: the standard Smagorinsky model with a classical log-law wall function, and the WALE model of Nicoud and Ducros [16] with a zero-velocity treatment at the walls.

For each ΔP case, a 600 mm long and 250 mm high sector of 33.7 mm in the spanwise direction is chosen so as to represent the entire flow (see Fig. 3). A grid sensitivity study was performed by Mendez and Nicoud [13] by investigating three different grids on the same hole diameter as in the present study. The controlling parameter for the mesh generation is the number of points along the hole diameter, defining the typical cell size within the hole. These authors showed that a typical cell size of 0.3 mm in the hole is sufficient to reproduce the main features of the flow considered. As a result, in the present work, the same cell size value of 0.3 mm in the holes is chosen to mesh the holes. This corresponds to $y^+ \approx 10$. Globally, the grid is composed of 10 million tetrahedral cells. The mesh is refined inside the holes and along the expected jets trajectories where strong turbulent activity occurs. Out of the expected cooling film location, the volume of the cells is linearly increased toward the boundaries of the domain (see Fig. 4).

As AVBP is an explicit compressible solver, the time-step Δt is determined through a CFL condition based on the maximum wave speed i.e. the sum of the convective flow velocity U and the sound speed c, namely:

$$\Delta t \leq CFL \left(\frac{\Delta x}{U + c} \right) \tag{1}$$

In order to reduce the computational time, the time-step can be increased by artificially decreasing the sound speed, expressed as:

$$c = \sqrt{\gamma r T} \tag{2}$$

T can be used as a variable to decrease the speed of sound, this technique is therefore referred to as *cryogenic calculation*. In order to keep density, momentum,

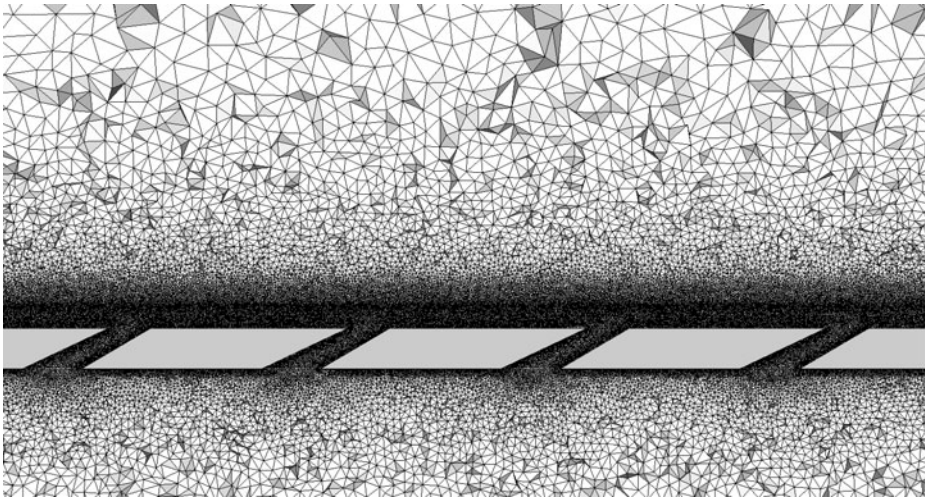

Fig. 4 Cut plane of the mesh around the holes

velocity and kinetic energy constant, the pressure is also modified according to the equation of state, the perfect-gas equation in the present case:

$$P = \rho r T \tag{3}$$

Before any modification, the Mach number in the upper channel is $M_0 = U_0/c_0 = 1.296 \times 10^{-2}$, with U_0 the mean flow velocity, and c_0 the sound speed taken at $T_0 = 300$K. The equivalent time-step following these parameters in the computation is thus $\Delta t_0 = 1.5 \times 10^{-7}$ s. The cryogenic Mach number M_{cryo} is taken as $M_{\text{cryo}} = 6 \times 10^{-2}$. This value is chosen sufficiently low so as to avoid any nonphysical compressibility effect.

The related sound speed is $c_{\text{cryo}} = 75$ m/s, and the new cryogenic temperature is $T_{\text{cryo}} = 14$ K. The atmospheric cryogenic pressure is decreased to $P_0 = 4{,}700$ Pa, but it is important to note that the pressure drop driving the blowing parameter $\mathcal{M}$ remains unchanged. Thus, for case 1, the pressure is equal to 4,700 Pa and 4,745 Pa in the upper and lower channel, respectively. Moreover, the Reynolds analogy is respected since the viscosity μ remains also unchanged. To achieve this, the reference temperature of the Sutherland law, relating for an ideal gas the dynamic viscosity μ to the temperature, is set to T_{cryo}. The equivalent time-step in the cryogenic computation is thus risen up to $\Delta t_{\text{cryo}} = 6.2 \times 10^{-7}$ s, corresponding to a simulation four times faster than the original one.

The conditions applied at the computational domain boundaries are represented in Fig. 5. The inlet condition for each channel is a mean turbulent velocity profile taken from the experimental data of Miron [14]. In the case of the WALE model, synthetic turbulence is also generated at both inlets following the technique of Kraichnan [11] and Smirnov [23]. Isotropic velocity fluctuations are superimposed onto the mean profile. The root mean square velocity (r.m.s) of the imposed fluctuations is chosen so as the represent 10% of the mean velocity. In all cases, the mean velocity profile at the inlet of the computational domain is strictly the same as the one measured in the experiment.

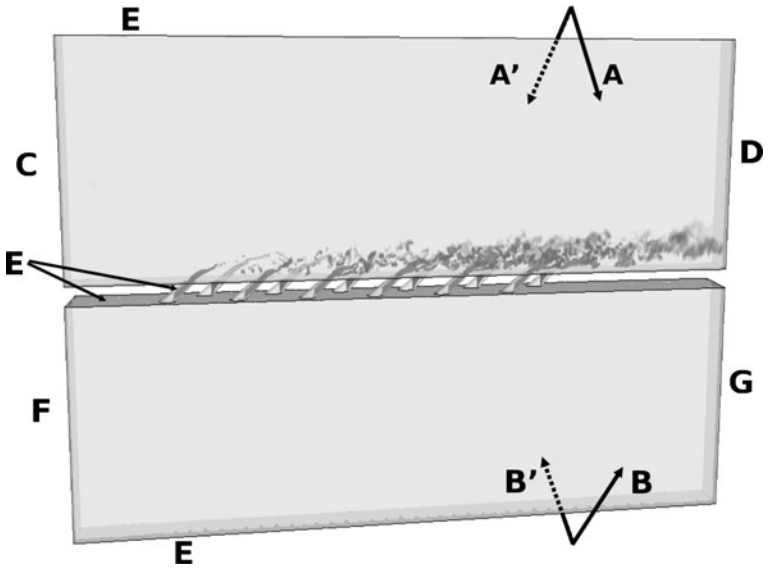

Fig. 5 Boundary conditions of the calculation domain: A-A' and B-B' show the periodic pair conditions; C and F point the inlet velocity conditions for the upper and lower channel, respectively; D and G point the outlet pressure condition for the upper and lower channel, respectively; and E, the wall condition. The domain is made transparent for visualization clarity

The atmospheric pressure is imposed at the outlet of the upper channel, but shifted by the cryogenic calculation as explained above. The flow is forced through the effusion holes by the imposition of a pressure drop across the plate. This pressure drop is strictly the same as imposed in the experiment (see Table 1). As a consequence, the pressure at the outlet of the lower channel is $P_{\text{atm}} + 45$ Pa for case 1, and $P_{\text{atm}} + 136$ Pa for case 2.

All solid surfaces (plate, holes and channel walls) are treated with the same wall model, which can be a no-slip condition or a log-law wall function. Periodic boundary conditions are taken between the faces delimitating the computational domain in the spanwise direction. The calculations are performed with the computational resources of CEA (French Atomic Energy Center). As an example, a physical time of 30 ms takes 24 h of wall clock time on 256 Intel Itanium, 1.6 GHz, double-core processors.

4 Results

As illustrated in Fig. 6, the whole vortical topology of the flow is close to the academical Jet-in-Cross-Flow studied by Fric and Roshko [8]. The main flow structure is the first counter-rotating vortex pair which dominates the wake of the jet. The jet shear-layer vortices resulting from the Kelvin–Helmholtz instability are clearly shown. A horseshoe vortex is observed just upstream of the hole, although this classical structure is weaker in the case of an inclined jet as mentioned by Mendez [13]. Very close to the wall, a secondary counter-rotating vortex pair is also observed.

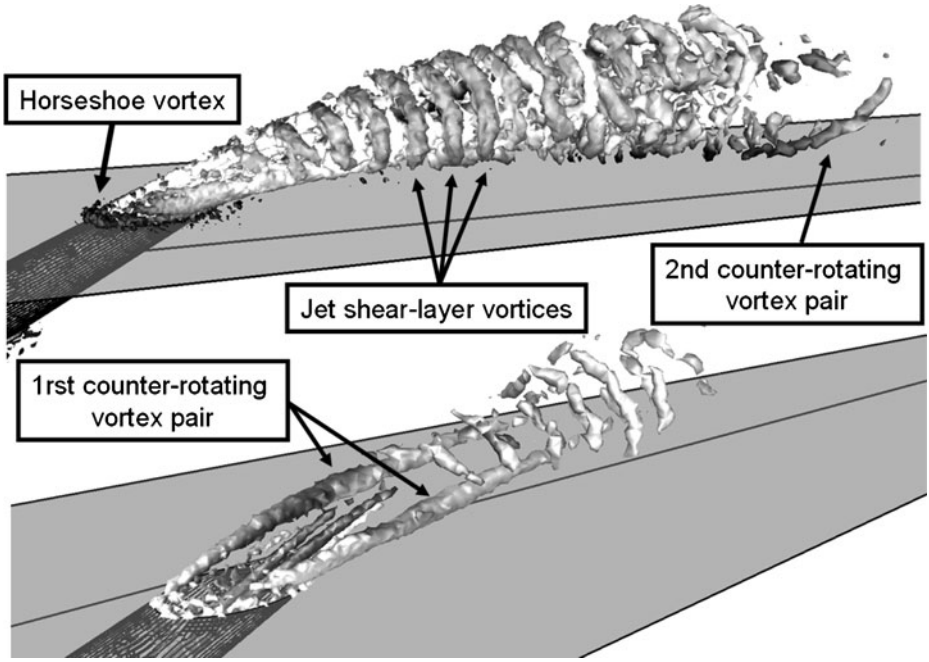

Fig. 6 Isosurface of two different values of Q-criterion showing the instantaneous structures of the flow. Values of Q-criterion are $1.5e^5$ for the upper picture and $1.5e^6$ for the lower picture, respectively

The following subsections will present experimental and LES results for cases 1 and 2. Values are given in a non-dimensional form by using the maximum velocity $U_{\max}$ in the upper channel and the channel height h as references. Profiles are taken at non-dimensional axial distances $x^* = x/d_{\text{ref}}$ downstream of the ninth hole axis, where d_{ref} is the reference hole diameter as explained in the experimental set-up section. W is the z-component of the velocity vector, i.e. the component normal to the jet exit section. For the Reynolds stress components, u' and w' are the velocity fluctuations in the x and z direction, respectively. For all graphs, PIV represents the experimental particle image velocimetry data of Most [15], LES1 stands for the results with a Smagorinsky model and a classical log-law wall function, LES2 corresponds to results obtained with a WALE model and a zero-velocity treatment at the walls, and LES3 denotes the results with a WALE model and a zero-velocity treatment at the walls with recourse to a synthetic turbulence injection.

In order to evaluate an appropriate averaging time of the LES computations, a flow-through time (FTT) is defined as being the characteristic time taken by a particle of the flow to cross completely an effusion-hole of the plate. Figure 7 shows for the LES1 method, a comparison of the mean axial velocity profile $U/U_{\max}$, the mean normal velocity profile $W/U_{\max}$, the r.m.s. axial velocity $\overline{u'}/U_{\max}$ and the r.m.s. normal velocity $\overline{w'}/U_{\max}$ for case 1 at $x^* = 5.92$, taken over an averaging time of 20 FTT, 40 FTT and 60 FTT, respectively. The mean and r.m.s velocity do not vary significantly with the averaging time, therefore the LES statistics are considered converged with an averaging over 20 FTT and this value is chosen in order to save computational time. For case 1, 20 FTT correspond to 40 ms of physical time.

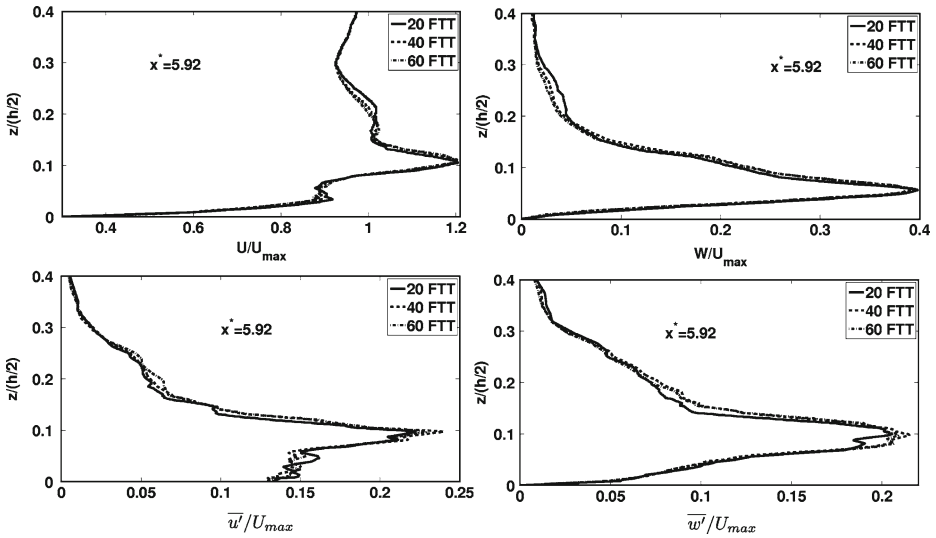

Fig. 7 Mean axial velocity profile $U/U_{\max}$, mean transversal velocity profile $W/U_{\max}$, axial root mean square velocity $\overline{u'}/U_{\max}$ and transversal root mean square velocity $\overline{w'}/U_{\max}$ for case 1 at $x^* = 5.92$ and for the LES1 method, and for an averaged time of 20 FTT, 40 FTT and 60 FTT, respectively

4.1 Case 1

Figure 8 presents the mean axial velocity profiles $U/U_{\max}$ and the mean normal velocity profiles $W/U_{\max}$ taken at $x^* = 2.92$ and $x^* = 5.92$, respectively. Figure 9

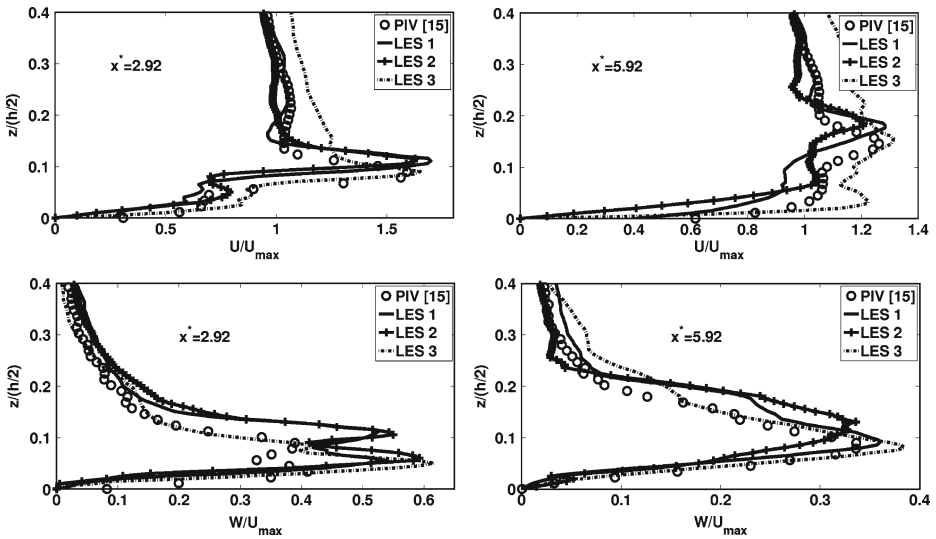

Fig. 8 Mean axial velocity profile $U/U_{\max}$ and mean transversal velocity profile $W/U_{\max}$ for case 1 at $x^* = 2.92$ and $x^* = 5.92$, respectively

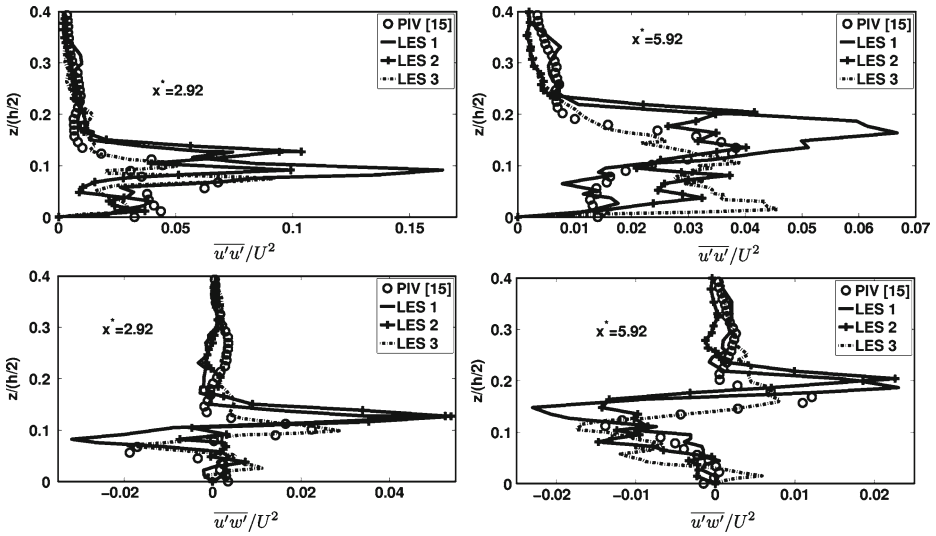

Fig. 9 Profiles of the Reynolds stress component $\overline{u'u'}/U^2$ and $\overline{u'w'}/U^2$ for case 1 at $x^* = 2.92$ and $x^* = 5.92$, respectively

shows profiles of the Reynolds stress components $\overline{u'u'}/U^2$ and $\overline{u'w'}/U^2$ at the same axial locations.

Globally, LES results are in good agreement with measurements and the whole flow is well recovered. Both models give a good amplitude level of the mean axial velocity but overestimate the mean normal velocity. With the Smagorinsky model, jets penetrate deeper in the upper flow than they do with the WALE model, but the synthetic turbulence injection brings a better concordance for the jet trajectory.

The same tendency can be observed for the profiles of the Reynolds stress components. The Smagorinsky model clearly overpredicts the normal component. Results obtained with the WALE model and turbulence injection are good for the $\overline{u'w'}$ component at each location and for both amplitude and spatial position.

As a whole, results for case 1 show that the models used for LES1 and LES3 (Smagorinsky model with a classical log-law wall function and WALE model with a zero-velocity treatment of the walls and with synthetic turbulence injection) provide better results than LES2. Therefore LES1 and LES3 will be the only two methods retained for the comparisons with the experimental results corresponding to case 2.

4.2 Case 2

Figure 10 shows the mean axial velocity profiles $U/U_{\max}$ and the mean vertical velocity profiles $W/U_{\max}$ taken at $x^* = 2.92$ and $x^* = 5.92$, respectively. Figure 11 presents the corresponding profiles of the Reynolds stress components $\overline{u'u'}/U^2$ and $\overline{u'w'}/U^2$ at the same axial locations.

For this case, results obtained with LES1 and LES3 are very similar. In both cases, the mean results are very close to the experimental values. The thickness of the film is slightly overestimated. The profiles of the Reynolds stress components exhibit a correct shape but the LES values are globally higher than the PIV ones.

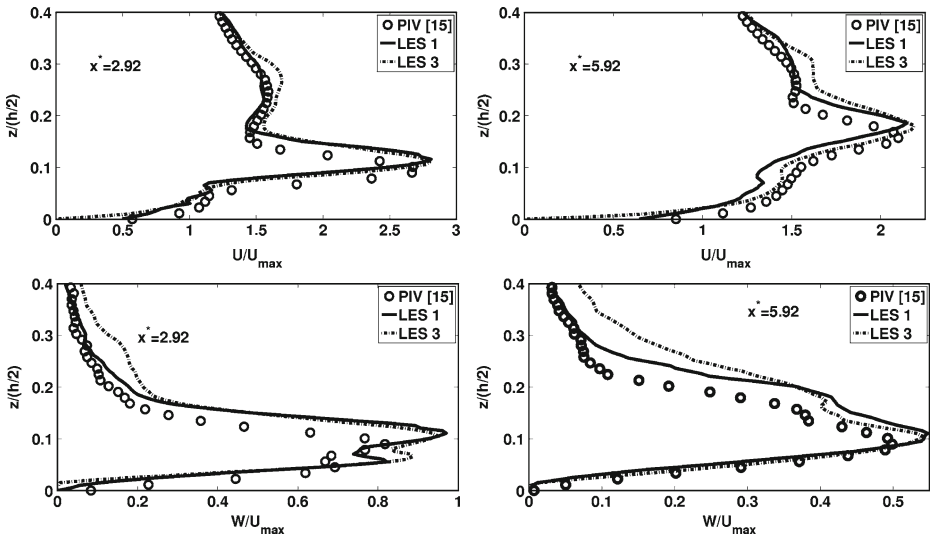

Fig. 10 Mean axial velocity profile $U/U_{\max}$ and mean transversal velocity profile $W/U_{\max}$ for case 2 at $x^* = 2.92$ and $x^* = 5.92$, respectively

Globally, these results are quite satisfactory and confirm that LES is an accurate tool to simulate the behaviour of the flow across an effusion-cooling plate. Based on this conclusion, the LES of the multi-perforated plate can now be used to study the interaction of the flow with an acoustic wave.

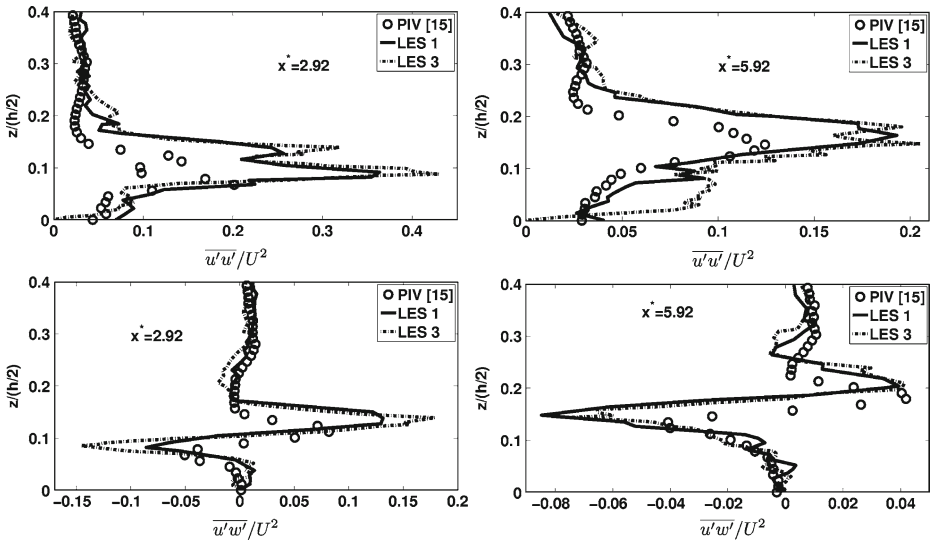

Fig. 11 Profiles of the Reynolds stress component $\overline{u'u'}/U^2$ and $\overline{u'w'}/U^2$ for case 2 at $x^* = 2.92$ and $x^* = 5.92$, respectively

5 Preliminary Investigation of the Acoustic Behaviour

As the integrity of a combustor may depend on the effectiveness of its effusion-cooling walls, a reliable homogeneous boundary condition model must reproduce the behaviour of the flow through a multi-perforated plate for different types of perturbations encountered during an engine operating cycle. In this section, the effect of a thermoacoustic instability is modelled by imposing a standing acoustic wave in the crossflow, i.e. in the upper channel of the calculation domain. Numerically, an acoustic fluctuation is superimposed to the flow conditions considered in the previous section.

The injection of velocity fluctuations in a mean flow is a well known problem in computational fluid dynamic. The easiest and most straightforward technique is to impose a fluctuating velocity at the inlet section, located here for convenience at $x_0 = 0$, namely:

$$u(x_0, t) = u_{\text{moy}} + u'(x_0, t) \tag{4}$$

with

$$u'(x_0, t) = u_0 \, e^{-j\omega t} \tag{5}$$

As shown by Kaufmann and Nicoud [10], this technique is not the best method to artificially produce an acoustic wave, because it also creates a convective, entropic wave that will introduce uncontrolled pressure waves and resonances. Indeed, as the computed flow is compressible, the velocity fluctuations resulting from waves traveling in the domain will interact with the forcing imposed at the boundary. The fluctuating velocity u' will still be equal to Eq. 5 and thus will act as a reflecting condition.

The proper forcing technique derives from the NSCBC [19] formulation. Physical variables such as velocity or pressure are reformulated into a characteristic form, allowing to separate incoming and outcoming waves at the surface boundary. Under these assumptions, the unsteady velocity at x_0 is:

$$u'(x_0, t) = \frac{1}{\rho_0 c_0}(A^+ - A^-)e^{-j\omega t} \tag{6}$$

where A^+ is the amplitude of the wave entering the domain and A^- the amplitude of the wave leaving the domain. The basic idea in order to introduce a real acoustic fluctuation around the mean flow is then to impose A^+ rather than to modulate $u'(x_0, t)$. So the ingoing wave train A^+ will cross the reflected wave train A^- at x_0 without interaction. This will ensure that the incoming wave is pulsated without interacting with the outgoing waves, and that no coupling between the inlet and the rest of the domain is possible. In other words, the surface boundary replicates an infinite tube at the inlet.

Following this theory, an incoming acoustic wave P'_{ac} is created on both sides (inlet and outlet) of the upper channel. Both waves have the same frequency and pressure amplitude. They are generated by imposing a velocity fluctuation and a pressure fluctuation at the inlet and outlet boundaries, respectively. In order to create a stationary acoustic mode, a natural frequency of the channel (255 Hz), obtained after a frequency sweep, is selected. The frequency of the acoustic pressure is chosen

so as to produce a spatial pressure distribution with a wavelength shorter than the cooling plate length.

The only influence of the cryogenic Mach number M_{cryo} onto the behaviour of the acoustic forcing is the modification of the natural frequency corresponding to the stationary mode selected. Since the goal of this study is to investigate the behaviour of a jet submitted to a stationary mode, any excitation frequency is acceptable as long as the mode is stationary. As the effect searched out is an uniformly pressure variation inside an effusion hole, only the frequency associated to this phenomena is influenced by the choice of a cryogenic computation.

As a result, some of the holes stand at or close to a pressure node while some others stand at or close to a pressure anti-node, which enables to study the response of the jets depending on the pressure signal they are submitted to. It must be highlighted that the ratio $P'_{ac}/\Delta P$ between the amplitude of the acoustic perturbation wave and the pressure difference across the effusion plate is one of the dominant physical parameters governing the response of the jets to the excitation. Basically, two types of interaction can be considered: for small values of $P'_{ac}/\Delta P$, the vortical flow topology can be altered by properly exciting the unstable modes of the jets, for large values, it can be expected that the acoustic wave will directly impact the whole jet structure. For intermediate values, these two mechanisms may coexist.

In order to illustrate the second regime of interaction, we shall consider here for case 1 ($\Delta P = 45$ Pa) a large value of $P'_{ac}/\Delta P$. The maximum pressure amplitude of the pulsation is set to $P'_{ac} = 800$ Pa. It must be noted that the ratio $P'_{ac}/\Delta P$ chosen here is high compared to values typically encountered in real combustors but still lies in a realistic range. Thus, the behaviour of a cooling flow submitted to such a pulsation provides valuable validation data to be used in an acoustic model of multi-perforated plate.

Figure 12 shows for the pulsated flow, a cut-plane at two differents instantaneous timesteps of the z-velocity component field. The pressure along the x-axis, at

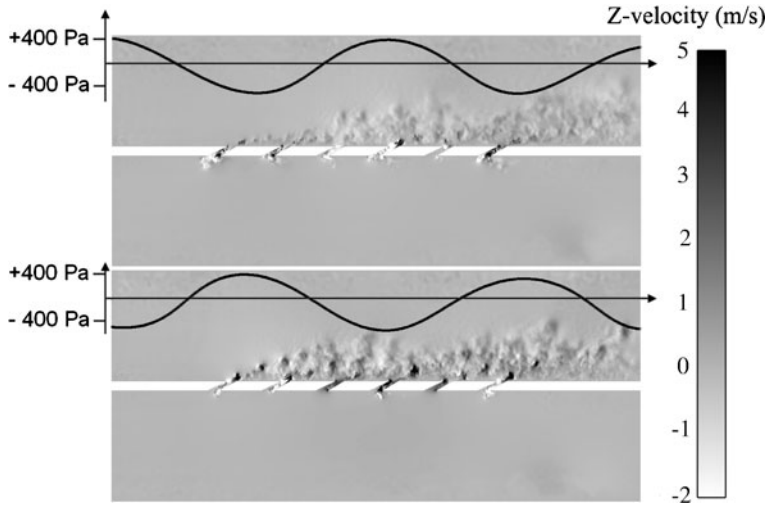

Fig. 12 Instantaneous z-velocity component with pressure surimposed and taken along the x axis

mid-channel height is also plotted to show the structure of the acoustic mode. The ±400 Pa pressure oscillations are relative to the outlet boundary pressure in the upper channel. Six jets are visible on this cut-plane of the even rows of the plate. The wavelength of the pulsation is approximately equal to the distance from the first to the sixth jet so that some of the jets are located at a pressure node (jets 3 and 5, corresponding to rows 6 and 10 of the whole plate) while other jets stand at a pressure antinode (jets 1 and 6, corresponding to rows 2 and 12 of the whole plate).

In the vicinity of a pressure node, the jets are weakly perturbed. On the contrary, the direction of the normal velocity of the jets located at an antinode is changing with the phase of the oscillation. When the pressure is at a maximum, the z-velocity is negative and jets are pulled back into the hole. When the pressure is at a minimum, the z-velocity is positive and larger than the one in the vicinity of a pressure node.

Figure 13 presents two mean z-velocity fields: one for the pulsated flow and one for its wave free counterpart. Both fields are averaged over a time equal to 20 oscillation periods. The comparison of these fields clearly shows that the trajectory of the jets is modified by the presence of the standing wave: forced jets flow further away from the channel wall than unforced jets and this effect is more pronounced on jets standing at a pressure anti-node. It can be inferred from this observation that the cooling of a wall could be weakened in the presence of such an acoustic wave in the crossflow.

The effect of the acoustic wave on the cooling performance of the plate can be further assessed a priori by analysing the mass-flow rate in one hole of each of the twelve rows for the cases with and without the standing wave in the crossflow, see Fig. 14. These values are calculated with the same averaged z-velocities as above. From the comparison, it clearly appears that the acoustic forcing has a strong blocking effect on the flow through the cooling holes. The total mass-flow rate in the pulsation-free case is 1.8 times as much as the one in the forced case. There is also a strong dispersion of mass-flow rate from one hole to another in the forced case, while the results obtained for the pulsation free case do not exhibit such a dispersion. As noted before, the stronger blocking effect is obtained for jets standing at a pressure anti-node (see, for example, rows 2 and 8). These observations show the potentially

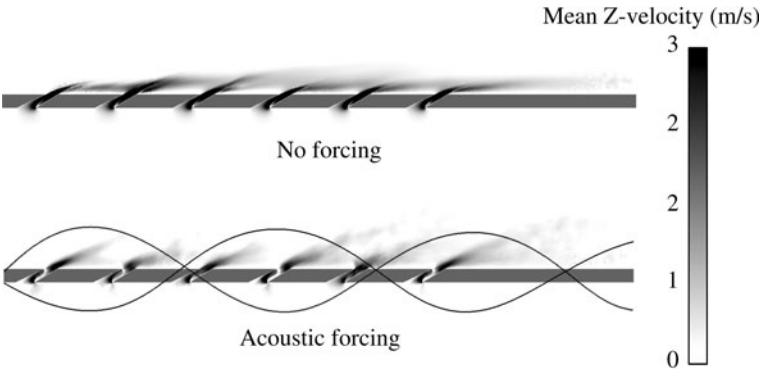

Fig. 13 Average z-velocity component for the acoustic forced case and the unforced case. For clarity, two phase-shifted acoustic pressure profiles are also shown

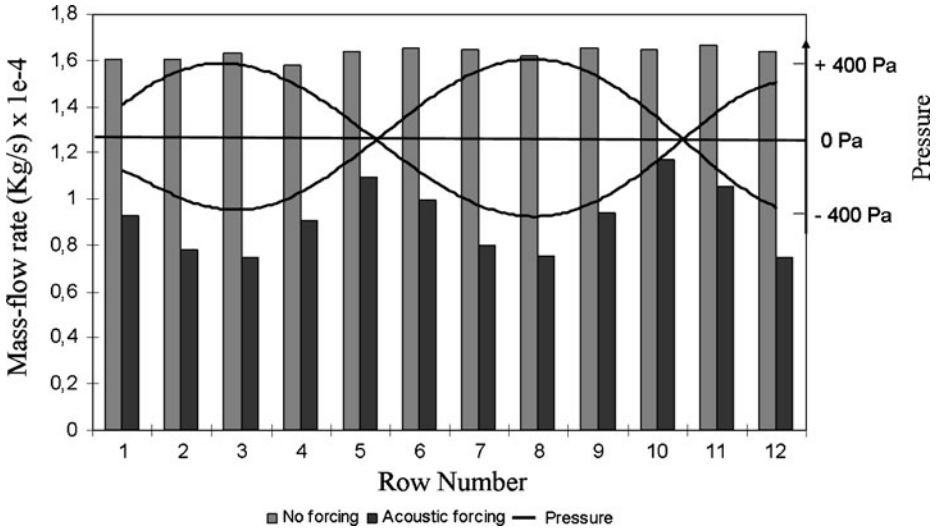

Fig. 14 Average mass-flow rate for each row of the plate and for both forced and unforced case

destructive effect that a strong acoustic wave may have on the flow around effusion-cooling wall.

It should be remembered though that this study was performed for the regime of interaction that occurs for large values of $P'_{ac}/\Delta P$. In an industrial context, when low values of $P'_{ac}/\Delta P$ are encountered, the forcing frequency becomes an important parameter. Indeed, as explained in the introduction section, there is a possibility to modify the vortical topology of coherent structures of the flow (see Fig. 6) by directly exciting (acoustically) the unstable modes of the jets. As shown in [21], JICF exhibit two types of unstable modes: one is associated with the shear-layer and the other one with the recirculation zone downstream of the jet hole. The response of shear layers to an acoustic excitation strongly depends on the relation between the acoustic forcing frequency f_f and the passage frequency of the vortical structures f_p. Indeed, turbulence can be generated or inhibited by pulsations with a forcing frequency comprised in the range of the passage frequencies of the vortical structures of the flow [9]. Although such a study is beyond the scope of the present work, we can illustrate though how its first step (i.e. determining f_p) can be carried out in the present configuration which differs quite significantly from the well-known academic configuration (i.e. normal jet in crossflow). Accordingly, two probes are placed in the jet of the first row for the unforced and forced case (see Fig. 15). One probe is located within the shear-layer (probe 1), one diameter downstream of the jet exit, along the jet trajectory. The second (probe 2) lies in the wake of the jet, near the wall.

Figure 16a and c show, for the first row and in absence of the acoustic wave, the time signals of the streamwise velocity component u, recorded by probes 1 and 2, respectively. A discrete Fourier transform of each signal is represented in Fig. 16b and d, respectively. The high-frequency peak at 851 Hz visible in the spectrum from probe 1 (Fig. 16b) is associated to the shear-layer. Concerning the probe 2 signals (Fig. 16d), the frequency spectra exhibit a low-frequency peak at 115 Hz associated with the jet-wake zone.

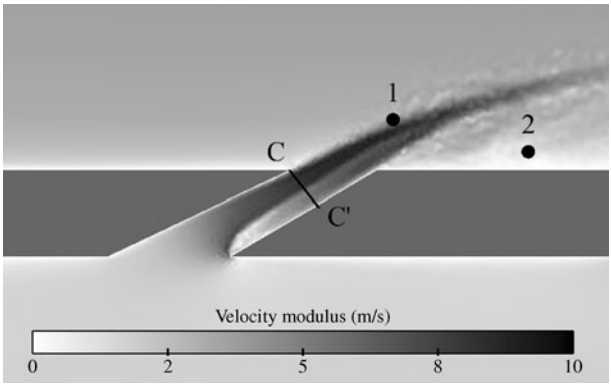

Fig. 15 Velocity field in the first row jet (m/s). Exit section definition (CC') and position of probes 1 and 2

The corresponding Strouhal numbers, defined as $S_t = \frac{f_p D}{\hat{U}_j}$, where f_p is the frequency, D is the diameter of the exit circular section CC' perpendicular to the hole axis (see Fig. 15) and $\hat{U}_j$ the mean velocity in CC' section, are found to be 0.66 and 0.09, respectively.

It is important to note that in the wake zone, probe 2 records another peak at the shear-layer frequency. As explained in [21], this phenomenon can be attributed

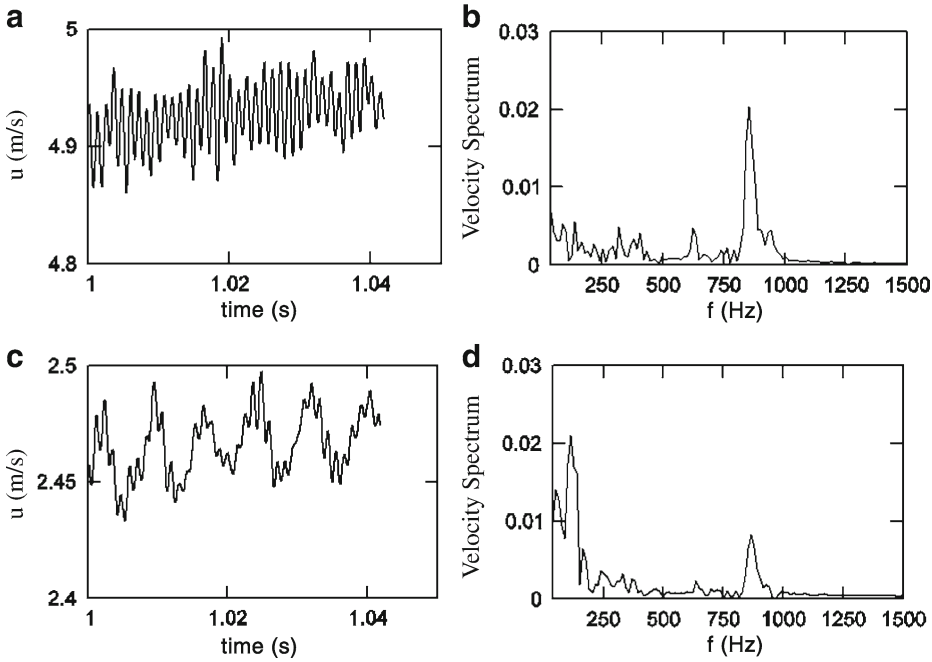

Fig. 16 Graphs **a** and **c**: Time signals of the streamwise velocity component u recorded for the unforced case by probes 1 and 2 in row 1, respectively. Graphs **b** and **d**: Discrete Fourier transform of time signals of probes 1 and 2, respectively

to up-right vortices that shed at the frequency of the shear-layer. For each formed shear-layer vortex an up-right vortex is created.

These results can be compared to those of Bagheri et al. [2, 21] for the academic JICF configuration, in the sense that they also found a high frequency peak associated with the shear-layer ($St = 0.17$) and a low frequency peak related to the wake zone ($St = 0.017$). The difference in the values of the Strouhal number can be associated with the difference of the Reynolds number values as well as of the jet inclination of the present configuration.

The time signals and associated frequency spectra of the streamwise velocity component u recorded at probes 1 and 2 for the forced case are shown in Fig. 17. Both the region of the shear-layer and the wake zone oscillate at the forcing frequency $f_f = 255$ Hz. No unstable mode appears to be excited and, as expected, the jet momentum perturbation dominates any other mechanism. The same behaviour is found for all jets, whatever their position with respect to the acoustic pressure distribution. To illustrate this, Fig. 18 shows the time signal and corresponding frequency spectrum provided by two axial velocity probes placed in the shear-layer and wake zone of the 5th row, i.e. close to an acoustic pressure node (see Fig. 14). Even if the value of $P'_{ac}/\Delta P$ effectively felt by the jet of row 5 is significantly smaller (the pressure amplitude at this location is $P'_{ac} \approx 200$ Pa) than the one at an anti-node, the jet oscillates with the same push-pull motion at the forcing frequency.

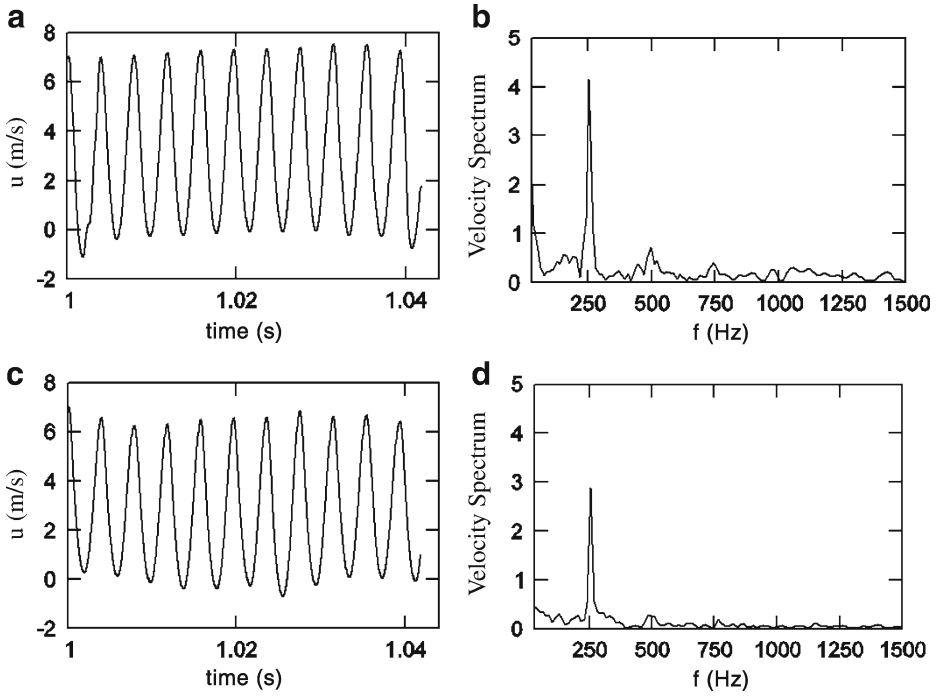

Fig. 17 Graphs **a** and **c**: Time signals of the streamwise velocity component u recorded by probes 1 and 2 in row 1 for the forced case, respectively. Graphs **b** and **d**: Discrete Fourier transform of time signals of probes 1 and 2, respectively

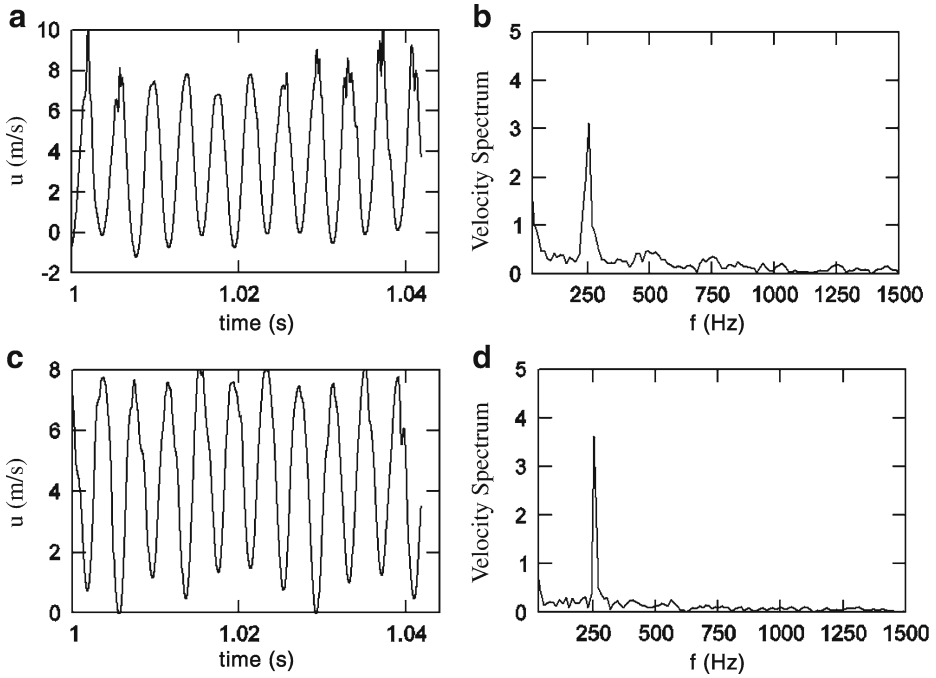

Fig. 18 Graphs **a** and **c**: Time signals of the streamwise velocity component u recorded by probes placed in row 5 (see text) for the forced case. Graphs **b** and **d**: Discrete Fourier transform of probes time signals

In Fig. 19, the signal issued from a control probe located in the middle of the upper channel, beyond reach of any jet flow influence, exhibits the same behaviour as that given by the previous probes. This shows that no interaction of the acoustic pulsation with the unstable modes of the jets is encountered in this configuration. A linear relationship between the mass-flow rate decrease in each jet and the corresponding

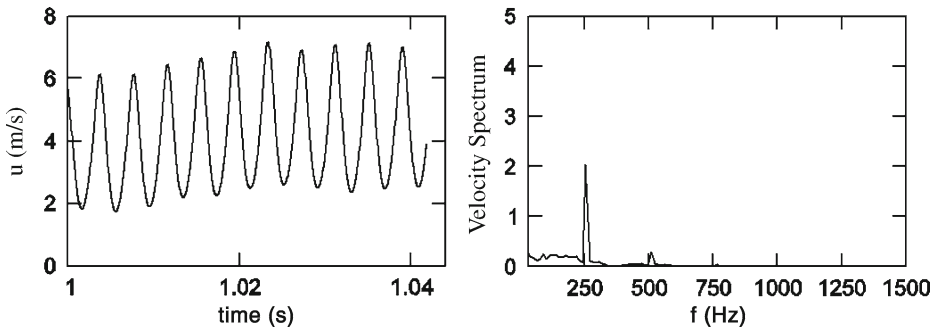

Fig. 19 Time signal of the streamwise velocity component u and associated Fourier transform recorded for a probe located in the middle of the channel (see text)

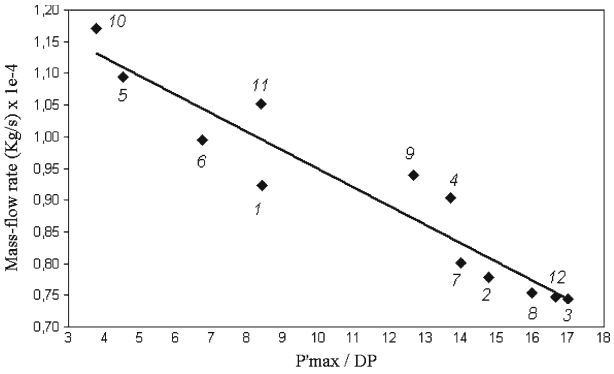

Fig. 20 Mass-flow rate as a function of $P'_{ac}/\Delta P$ and corresponding row numbers

value of $P'_{ac}/\Delta P$ is found by plotting these variables for all rows of the calculation domain (see Fig. 20). It can be therefore concluded that the mass-flow rate decrease in the effusion-cooling plate is entirely due to the pressure loss resulting from the push-pull motion imposed to the jets.

6 Future Investigations and Conclusions

This study is a first attempt to determine the impact that a standing acoustic wave may have on the flow through the effusion-cooling walls of an aeronautical combustor. It has been shown that a stationary acoustic mode can be potentially destructive, since it severely reduces the flow rate through the cooling holes. The values of the acoustic pressure investigated lie in the upper range of real acoustic pressure found in combustors.

In this range of values, it has been shown that the flow-blocking effect is entirely due to an increased pressure loss in the plate. Parametric studies are still needed to determine more precisely the range of application of this effect and whether non-linear interactions between acoustic pulsation and unstable modes of the jets are to be expected.

From a numerical point of view, it has been shown in this study that LES can be an accurate tool to model such a wall-bounded flow. The results depend on the numerical strategy adopted and the WALE subgrid-scale model with synthetic turbulence injection gives very satisfactory results.

Acknowledgements This study is part of the 4-year KIAI project started in May 2009, which is a European initiative financed under the FP7 and addresses innovative solutions for the development of new combustors in aero-engines. It aims at providing low NOx methodologies to be applied to design these combustors.

The research leading to these results has received funding from the European Community's Seventh Framework Programme (FP7/2007-2013) under Grant Agreement ACP8-GA-2009-234009.

The financial support of the French *Agence National de la Recherche Technique* is gratefully acknowledged.

The authors wish to thank Laurent Gicquel for fruitful discussions about LES of wall-bounded flows.

References

1. Baggett, J.S., Jiménez, J., Kravchenko, A.G.: Resolution requirements in large-eddy simulations of shear flows. In Annu. Res. Briefs, Center Turbul. Res., Stanford Univ, pp. 51–66 (1997)
2. Bagheri, S., Schlatter, P., Schmid, P.J., Henningson, D.S.: Global stability of a jet in crossflow. J. Fluid. Mech. **624**, 33–44 (2009)
3. Boileau, M., Staffelbach, G., Cuenot, B., Poinsot, T., Bérat, C.: LES of an ignition sequence in a gas turbine engine. Combust. Flame **154**(1–2), 2–22 (2008)
4. Chapman, D.R.: Computational aerodynamics, development and outlook. AIAA J. **17**, 1293–1313 (1979)
5. Colin, O., Rudgyard, M.: Development of high-order Taylor Galerkin schemes for unsteady calculations. J. Comput. Phys. **162**(2), 338–371 (2000)
6. Crighton, D.G., Gaster, M.: Stability of slowly diverging jet flow. J. Fluid. Mech. **77**(2), 397–413 (1976)
7. Crow, S.C., Champagne, F.H.: Orderly structure in jet turbulence. J. Fluid. Mech. **48**(3), 547–591 (1971)
8. Fric, T.F., Roshko, A.: Vortical structure in the wake of a transverse jet. J. Fluid Mech. **279**, 1–47 (1994)
9. Ho, C.M., Huerre, P.: Perturbed free shear layers. Ann. Rev. Fluid. Mech. **16**, 365–424 (1984)
10. Kaufmann, A., Nicoud, F., Poinsot, T.: Flow forcing techniques for numerical simulation of combustion instabilities. Combust. Flame **131**(4), 371–385 (2002)
11. Kraichnan, R.H.: Diffusion by a random velocity field. Phys. Fluids **13**, 22–31 (1970)
12. Megerian, S., Davitian, J., Alves, L.S., Karagozian, A.R.: Transverse-jet shear-layer instabilities. Part 1. Experimental studies. J. Fluid. Mech. **593**, 93–129 (2007)
13. Mendez, S., Nicoud, F.: Large-eddy simulation of a bi-periodic turbulent flow with effusion. J. Fluid Mech. **598**, 27–65 (2008)
14. Miron, P.: Etude Expérimentale des Lois de Parois et du Film de Refroidissement Produit par une zone Multiperforée sur une Paroi Plan. PhD Thesis, Université de Pau et des Pays de l'Adour (2005)
15. Most, A.: Etude Expérimentale et Numérique du Film de Refroidissement Produit par l'Injection Pariétale d'Air au Travers d'Une Paroi Multiperforée. PhD Thesis, Université de Pau et des Pays de l'Adour (2007)
16. Nicoud, F., Ducros, F.: Subgrid-scale stress modelling based on the square of the velocity gradient tensor. Flow Turbul. Combust. **62**(3), 183–200 (1999)
17. Nicoud, F., Baggett, J., Moin, P., Cabot, W.: LES wall-modeling based on optimal control theory. Phys. Fluids **13**(10), 2968–2984 (2001)
18. Piomelli, U., Balaras, E.: Wall-layer models for large-eddy simulations. Annu. Rev. Fluid Mech. **34**, 349–374 (2002)
19. Poinsot, T., Lele, S.: Boundary conditions for direct simulations of compressible viscous flows. J. Comput. Phys. **101**(1), 104–129 (1992)
20. Prière, C., Gicquel, L.Y.M., Gajan, P., Strzelecki, A., Poinsot, T., Bérat, C.: Experimental and numerical studies of dilution systems for low emission combustors. AIAA J. **43**(8), 1753–1766 (2005)
21. Schlatter, P.J., Bagheri, S., Henningson, D.S.: Self-sustained global oscillations in a jet in crossflow. Theor. Comput. Fluid Dyn. **25**(1–4), 129–146 (2010)
22. Smagorinsky, J.: General circulation experiments with the primitive equations: I. The basic experiment. Mon. Weather Rev. **91**, 99–164 (1963)
23. Smirnov, A., Shi, S., Celik, I.: Random flow generation technique for large eddy simulations and particle-dynamics modeling. J. Fluids Eng. **123**, 359–371 (2001)
24. Templeton, J.A., Moin, P., Wang, M.: Wall models for Large-Eddy simulation based on optimal control theory. Report No. TF-98, Stanford University (2006)
25. Wolf, P., Staffelbach, G., Roux, A., Gicquel, L., Poinsot, T., Moureau, V.: Massively parallel LES of azimuthal thermo-acoustic instabilities in annular gas turbines. C. R. Mécanique **337**, 385–394 (2009)